ANALYSIS OF DATA OF THE 1968-69 AIRBORNE AURORAL EXPEDITIONS

Final Report

S. B. Mende

March 1973

Prepared Under Contract
No. NAS2-7296

By

Lockheed Palo Alto Research Laboratory
3251 Hanover Street
Palo Alto, California 94304

For

Ames Research Center
National Aeronautics and Space Administration
Moffett Field, California

OBJECTIVE

This is a report summarizing the findings of contract NAS2-7296.

INTRODUCTION

Two auroral expeditions were flown by NASA on the CV 990 aircraft. The subject of this contract was the further reduction of the data of the airborne photometer on the CV 990 to investigate two specific problems.

a. Coordinated auroral particle and optical observations.

b. Substorm effects in auroral spectra.

To preserve the technical unity of this report, we have included contributions from Dr. R.H. Eather of Boston College who has been funded under a different contract.

PUBLICATIONS

a. The substorm related data analysis results will be published under the title: "Substorm Effects in Auroral Spectra." This will be submitted shortly to J. Geophys. Res.

b. Coordinated measurements of optical aurora with OV1-18 satellite will be presented by Dr. S.B. Mende as an invited paper at the Aurora-Airglow Symposium at the General Scientific Assembly in Kyoto, Japan. The paper will also be subsequently published as part of a collection of papers in the form of a book.

Chapter I

COORDINATED AURORAL PARTICLE AND OPTICAL OBSERVATIONS

Introduction

On the 8th of December, 1969 the NASA airborne auroral expedition CV990 airplane was flown under the predicted trajectory of the OV1-18 satellite. The pre-planned experiment permitted the coordinated observation of the same aurora by the Lockheed photometer on the CV990 aircraft and the Lockheed auroral particle instrumentation on the OV1-18 satellite. The subsatellite point as projected to the 100 km altitude and the photometer field of view coincided at 1017:11 in longitude (256.87°E) and at 1017:14 at the same geodetic latitude (59.58°N). The closest approach occurred at about 1017.13 UT and the distance between the center of the photometer field of view and the subsatellite point was less than 7 km. The satellite and the airplane were moving in a parallel trajectory 18° West of South.

The satellite was tumbling and the detector pitch angle was varying during the observation. Because of this the interpretation of the results is not straightforward.

In previous publications, Eather and Mende (1972) have been able to interpret auroral photometric measurements in terms of statistical properties of proton flux, electron energy flux and mean energy of electron precipitation. Quite considerable assumptions were built into these interpretations as regards to electron energy spectrum, pitch angle distribution and upper atmospheric reaction modeling. The single case of these coordinated results is treated here using these same assumptions to examine their validity hold in this particular coordinated case.

Protons

Flux levels were low, and the CMP 3A (0.4 - 1.2 kev) detector and all integral flux detectors (> 7 kev) were at background levels. Only two differential detectors, CMP-3B (0.88- 2.6 kev) and CMP-3C (2.9 - 8.7 kev) responded, and the outputs from these detectors is plotted in Fig. 1. Also shown is the corresponding detector pitch angle (the satellite was tumbling).

It may be seen that the detectors responded only when looking up the field lines, which is to be expected as one expects little backscatter of the proton flux. Thus, the latitude extent of proton precipitation was probably larger than that of detector response, as it would be unreasonably fortuitous for the proton precipitation to locate just in the region when the detectors were looking up the field lines.

On the assumption that the proton precipitation is reasonably stable, we can get an idea of the latitude distribution of the proton precipitation from the latitude profile of the proton arc measured from the aircraft. Although charge-exchange effects will broaden the arc, it is clear from Fig. 1 that the satellite response was some 1-2^{o} south of the real maxima in proton flux, and that the satellite detectors were looking down the field lines when passing over the region of peak precipitation.

Thus, we cannot do a complete coordination analysis that takes satellite proton spectra as functions of latitude, and then calculates the expected proton arc distribution after allowance for charge-exchange spreading.

But it is of interest to calculate the expected Hβ emission corresponding to the peak satellite fluxes. At this time the detectors were looking at a pitch angle of 130° (downward 50° from the field line); the calculation will assume isotropy over the loss cone. The satellite was at 535 km, which is above the average height for a first charge-exchange collision, so no correction is necessary for a partly equilibrated beam.

Fig. 2 shows proton spectral data near peak satellite response. The 0.4 - 1.2 kev detector gives an upper limit. A conservative upper limit is obtained for the > 7.7 kev integral detector by assuming all of any flux is in the range < 12 kev. One could draw a variety of curves through the plotted flux levels, though the two curves plotted in Fig. 2 seem to represent limits for any reasonably smoothly varying curves.

Using cross sections published by Eather (1967), we calculated the expected Hβ emission for the two curves as 7.0R for spectrum A and 10.7R for spectrum B. Charge-exchange spreading should be considered, and although we do not have the complete latitudinal distribution of proton precipitation above the atmosphere (which is necessary to calculate the resultant proton arc distribution), it is useful to consider a previous analysis where such data were available. Fig. 3 shows the results of such an experiment from an OVI-18 pass over College, Alaska. The dashed curve (for > 7.5 kev detector) is representative of the latitudinal distribution of the proton flux;

the resultant Hβ emission, calculated from complete spectral information and with charge-exchange considered, is similar in shape to the Hβ curve in Fig. 1. Thus, by analogy, we arrive at a rough correction for charge-exchange, and conclude the measured Hβ intensity near peak satellite response (on the high latitude wing of the curve) would be about 50% higher than in the absence of charge-exchange spreading of protons from near the peak of the flux distribution.

This gives a theoretical zenithal Hβ intensity of ~ 10R for spectrum A and ~ 16R for spectrum B; the measured intensity was 6R. In view of the large uncertainties in cross section data used (see discussion by Eather, 1967), especially at these low energies, the agreement is satisfactory.

Miller and Shepherd (1969) have advanced arguments favoring a different cross-section curve for Hβ emission than that adopted by Eather (1967) and used here. Their curve gives much higher cross-sections at low proton energies. Using the Miller-Shepherd cross-sections in the above calculations gives an expected Hβ emission of ~ 31R for spectrum A and ~ 53R for spectrum B, much higher than the measured 6R. It would seem the cross-sections postulated by Miller and Shepherd are far too high at low energies.

The final point one can make from this coordination is a comment about the upward-going proton flux at 535 km. As the detector pitch angle sweeps through 90° at a satellite time of 905301 and begins to look down the field

lines, the satellite is moving into a region of weaker precipitation. Yet the measured flux is at background level by 905304, indicating that any upward proton flux is confined to within 5° of flat pitch angles.

Electrons

There was low-level electron precipitation present at the time of the overpass, but the flux levels were such that zenithal emissions were well below visual or all-sky camera thresholds. The photometric records show that at the time of overpass, spectral intensities were steady. Two to four minutes before the overpass, and again 3-6 minutes after the overpass, weak pulsating aurora was recorded (quasi-period $\sim$ 5 secs).

Unlike proton precipitation, it is not reasonable to assume the electron precipitation was steady as a function of latitude and time, especially as we know some pulsation activity was present. Hence, the only meaningful coordination analysis is to study the exact point of coordination.

In Table 1 we list the measured zenithal intensities of the five emissions being monitored. The airglow corrections to λ5577 and λ6300 were obtained by averaging the λ5577 and λ6300 intensities during the last period the λ4278 fell to zero before the coordination (0856 UT when I(5577) = 94R, I(6300) = 57R) and the first period λ4278 fell to zero after the coordination (1056 UT when I(5577) = 60R, I(6300) = 58R). The corrections to the total intensity for proton excitation are the same as those used in all our previous statistical analyses (Eather and Mende, 1971, 1972) and represent an average figures determined for proton excitation (Eather, 1967).

Table 1

λ	Total Intensity (R)	Airglow Correction (R)	Proton Correction (R)	Electron Excitation (R)
4278	79.	0	37.	42.
Hβ	12.5	0	12.5	0
5200	5.1	1.7		
5577	590.	77.	125.	388.
6300	152.	57.	31.	64.

Ratios for electron excitation: 6300/4278 = 1.52

6300/5577 = 0.16

5577/4278 = 9.2

From the electron excited λ4278 N_2^+ intensity, and the 6300/4278 ratio, we can determine the energy spectral parameter α for an assumed spectral shape of $N(E)\,dE = Ee^{-E/\alpha}\,dE$ and using Rees (1970) theoretical calculations. From these theoretical curves for this coordination, we deduce α = 1.6 keV, corresponding to an average energy for the spectrum of 3.2 keV. The total electron energy influx is given by the λ4278 N_2^+ intensity, using a conversion of 280R/erg $cm^{-2}sec^{-1}$, and is 0.15 ergs/cm^2sec, or 0.05 erg/cm^2sec ster if isotropy is assumed.

Comparison with the satellite measurements of electron fluxes is again made difficult by the fact that the satellite was tumbling, so that one group of detectors (CME2A, 3B, 3C and 3D) were looking down the field lines

at an upcoming pitch angle of 110°, and a second group (CME1A-E) were looking at an upcoming pitch angle of 156°. The particle pitch angle is defined by the zero angle looking up along the field line. The flux levels for the second group were at background level at the time of overpass, indicating that the backscattered flux was confined to pitch angles $< 156^{\circ}$.

The integral flux (0.8 - 16.3 keV) and average electron energy (from the CME2A, 3B, 3C and 3D detectors), and pitch angle of data acquisition, are shown in Fig. 4 for times near the overpass. The gradual change in flux as the detectors leave the loss cone and begin sampling upcoming flux suggests that the backscattered flux in this region was comparable to the downgoing flux. The average energy at overpass was 4.0 keV, a little higher than deduced photometrically (3.2 keV). (Note however that 5 secs either side of the overpass time, the average electron energy measured by the satellite was $\sim$ 3.5 keV.) The total energy backscattered at 110° as measured by the satellite was 0.07 ergs/cm^{2}sec ster, compared to 0.05 erg/cm^{2}sec ster deduced photometrically (on the assumption of isotropy).

The assumption of isotropy is generally reasonable as long as the electron flux is above 10^6 cm^{-2}sec^{-1}ster^{-1} keV^{-1} (Paschman et al., 1972). Using the isotropy assumption and energy spectrum which satisfies the optical measurements, one can derive the upcoming backscatter spectrum as a function of pitch angle (Walt et al., 1968).

The assumed downcoming isotropic energy spectrum is of the form:

$$N(E)\,dE = 1.1 \times 10^7\, E\, e^{-E/1.6}\, dE \text{ ster}^{-1}\text{cm}^{-2}\text{sec}^{-1},$$

where E is in keV.

This spectrum was fed into a computer program(by courtesy of W. Francis) that calculates the backscatter spectrum at various pitch angles (Walt et al., 1968).

The calculated backscattered spectrum at various computed pitch angles is shown in Fig. 5. There is remarkably good agreement between the calculated spectra at about 110° and the measured fluxes in the detectors. Note that the curves also predict that the backscattered fluxes should be at detector background level at 156°, accounting for the lack of the flux observation with these detectors.

Background windows were indicated by the broken line energy windows.

Conclusions

Using the coordinated data from OV1-18 satellite and the airborne photometer experiment on the 8th of December 1969, direct comparisons could be made between the particle fluxes and the optical auroral emissions.

With the assumption that the proton precipitation was fairly time invariant, the hydrogen arc observed by the aircraft photometer could be compared to the proton precipitation by the satellite proton detectors. By assuming isotropic pitch angle distribution and by using the charge exchange correction from another coordinated case, the Hβ emission intensities could be made to agree with the proton flux input, provided the earlier (Eather, 1967) Hβ emission cross sections were used.

In the electron case, direct comparison was possible at the time of closest coordination. Using the optical data the electron energy flux and mean energy could be derived according to technique of Eather and Mende (1972) from the precipitating downcoming flux.

A simple spectrum and isotropic pitch angle distribution which satisfy the optical observations was assumed and this was used to calculate the upward coming backscatter fluxes. These calculated spectra were compared directly to the satellite measurements of the various downward looking energy channels and very good agreement was found.

Figure Captions

Figure 1 Proton detectors CMP 3A and CMP 3B and CMP 3C response and pitch angle of the detectors (0° upcoming particle, 180° down going particles). The CV990 airplane Hβ photometer data is also shown as a function of latitude.

Figure 2 Proton spectral distribution near peak satellite fluxes.

Figure 3 Coordinated observation of proton arc near College with meridian photometer and the OV1-18 satellite. Photometer zenith angles are indicated.

Figure 4 Integral flux (0.8 - 16.3 keV) and average electron energy (from CME 2A, 3B, 3C and 3D detectors) and the pitch angle of measurement (0° upcoming particle, 180° down going particles). The time of coordination is shown with the broken vertical line.

Figure 5 The backscatter fluxes at 535 km due to a downward isotropic flux of electrons whose spectra is given by:

$N(E)\,dE = 1.1 \times 10^{7}\, E \exp(-E/1.6)\, dE$ cm^{-2}sec^{-1}ster^{-1}, where E is in keV. This spectrum satisfies the optical ratio measurements and yields a mean energy $\bar{E} = 3.2$ keV and total energy flux of 0.05 erg cm^{-2}sec^{-1}ster^{-1}.

Satellite energy windows and flux levels with detector backgrounds are also superimposed.

References

Eather, R.H.; "Auroral Proton Precipitation and Hydrogen Emissions," Reviews of Geophysics, 5, 207, 1967.

Eather, R.H. and S.B. Mende; "Airborne Observations of Auroral Precipitation Patterns," J. Geophys. Res., 76, 1746, 1971.

Eather, R.H. and S.B. Mende; "Systematics in Auroral Energy Spectra," J. Geophys. Res., 77, 660, 1972.

Miller, J.R. and G.G. Shepherd; "Rocket Measurement of H Beta Production in Hydrogen Aurora," J. Geophys. Res., 74, 4987, 1969.

Paschmann, G., R.G. Johnson, R.D. Sharp and E.G. Shelley; "Angular Distribution of Auroral Electrons in the Energy Range 0.8 to 16 keV," J. Geophys. Res., 77, 6111, 1972.

Rees, M.H.; Private communication, 1971.

Walt, M., W.M. MacDonald and W.E. Francis; "Penetration of Auroral Electrons into the Atmosphere," Physics of the Magnetosphere, ed. R.L. Carovillano, pp. 534-555, 1968.

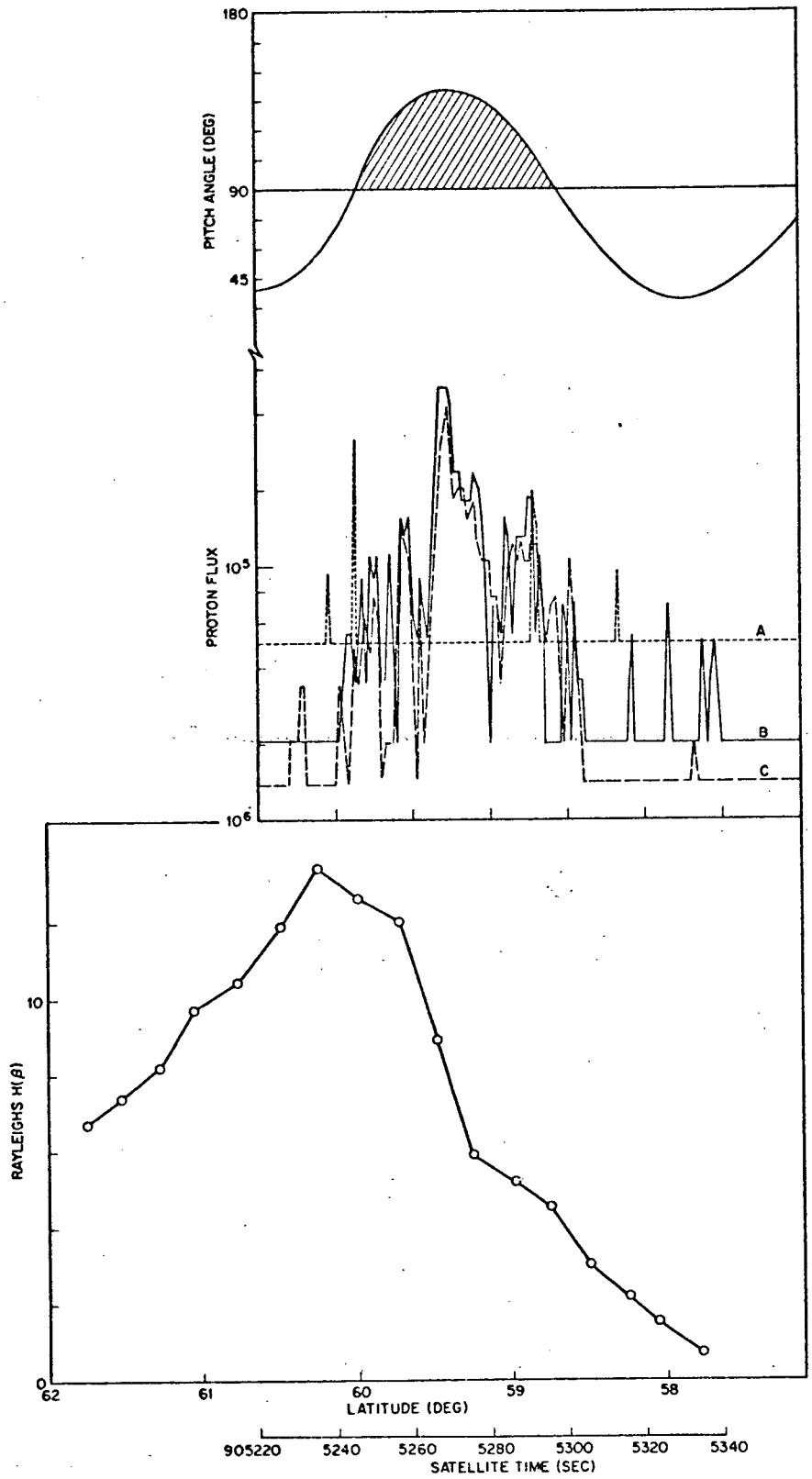
180
90
45
PITCH ANGLE (DEG)
10^5
10^6
PROTON FLUX
A
B
C
10
0
RAYLEIGHS H(β)
62
61
60
59
58
LATITUDE (DEG)
905220
5240
5260
5280
5300
5320
5340
SATELLITE TIME (SEC)

Figure 1

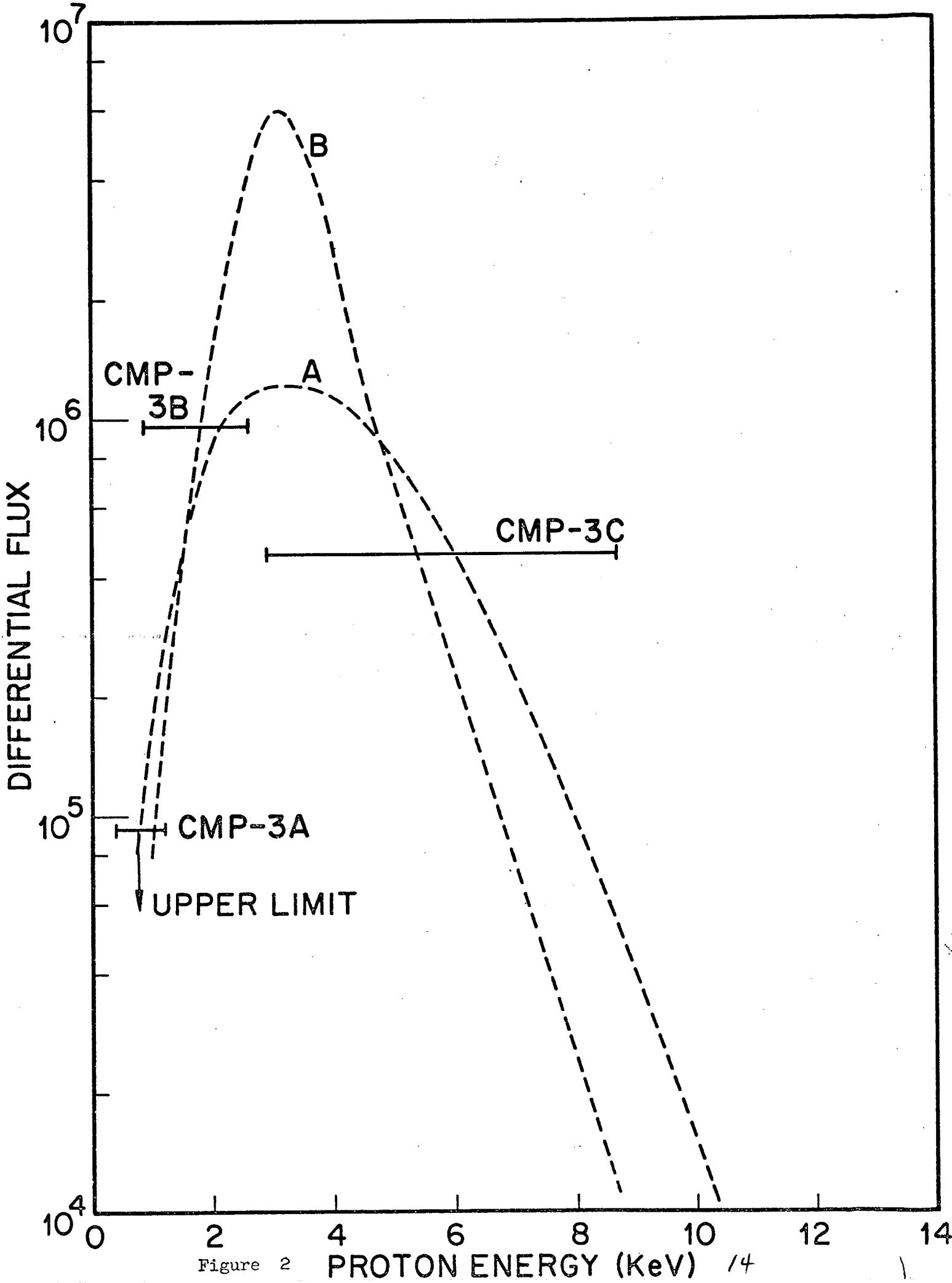
10^7
10^6
10^5
10^4
DIFFERENTIAL FLUX
B
A
CMP-3B
CMP-3C
CMP-3A
UPPER LIMIT
0
2
4
6
8
10
12
14
PROTON ENERGY (KeV)

Figure 2

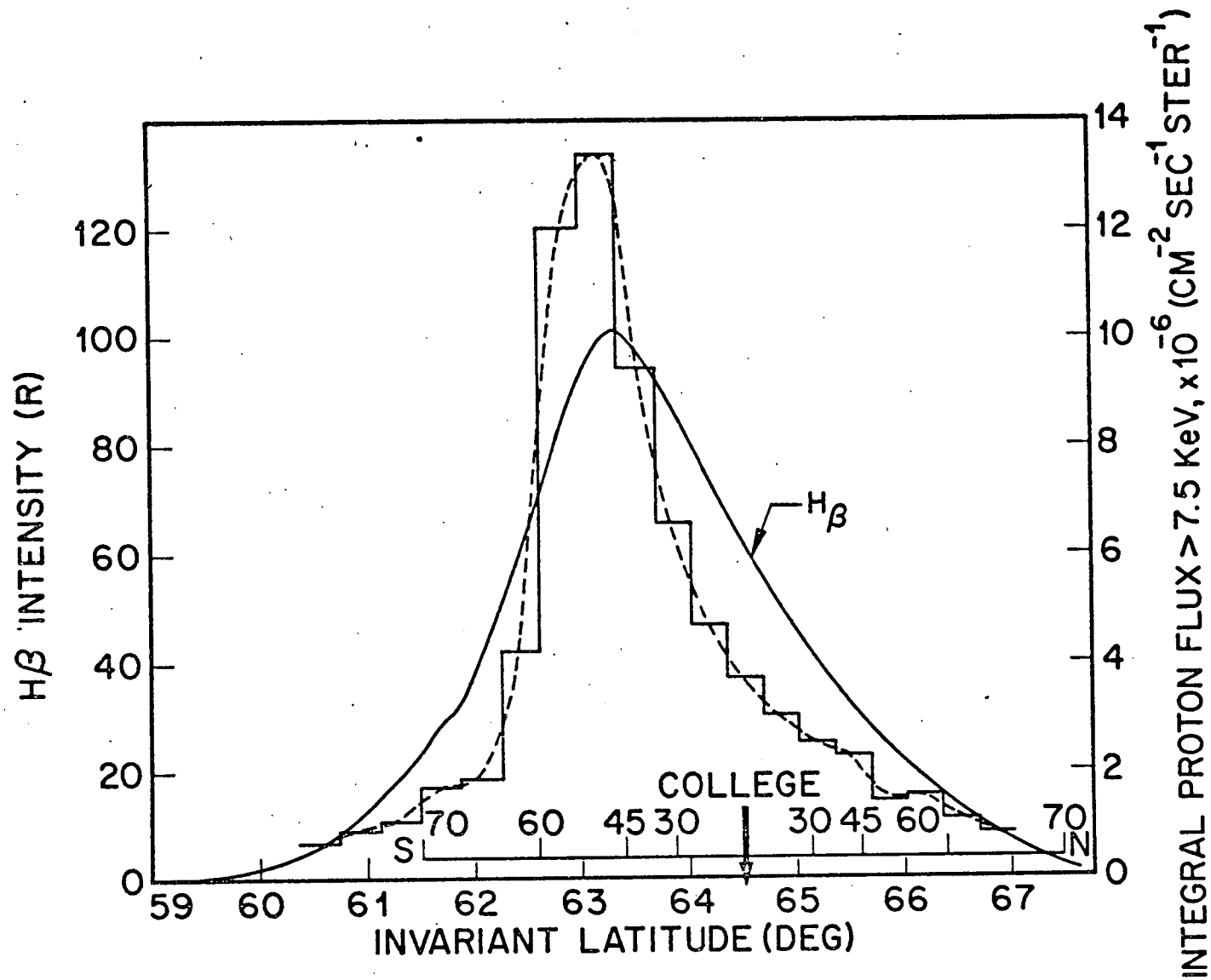
Hβ INTENSITY (R)
INTEGRAL PROTON FLUX > 7.5 KeV, x10⁻⁶ (CM⁻² SEC⁻¹ STER⁻¹)
INVARIANT LATITUDE (DEG)
Hβ
COLLEGE
S
N
70 60 45 30
30 45 60 70
0 20 40 60 80 100 120
0 2 4 6 8 10 12 14
59 60 61 62 63 64 65 66 67

Figure 3

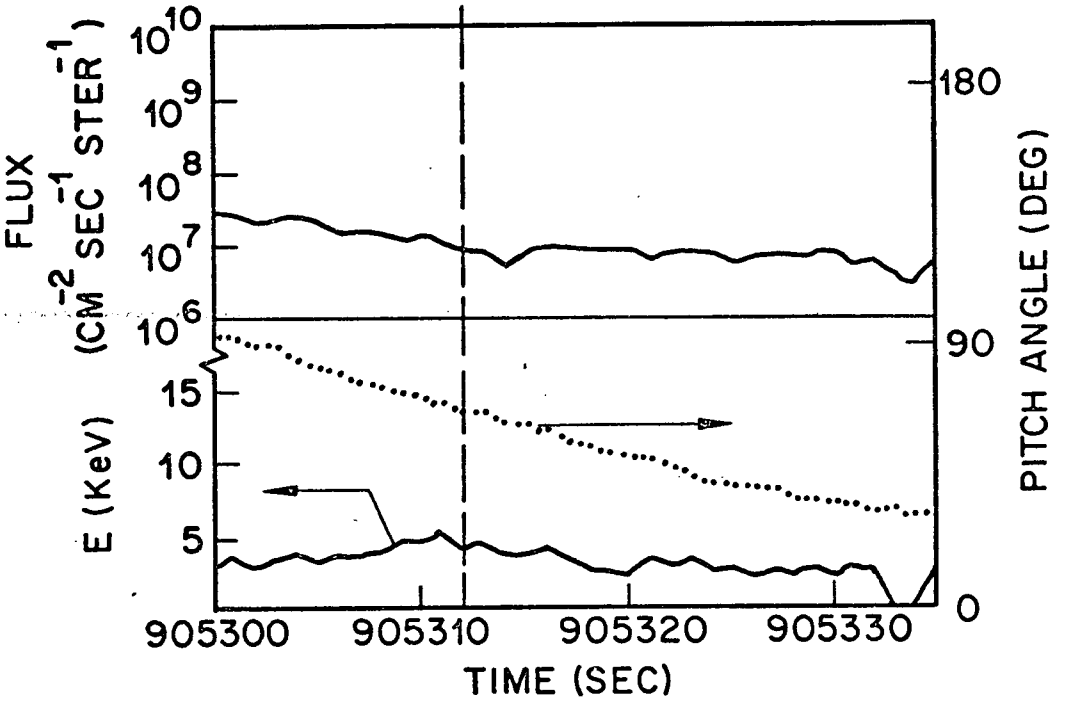
FLUX
(CM^{-2} SEC^{-1} STER^{-1})
10^{10}
10^{9}
10^{8}
10^{7}
10^{6}
15
10
5
E (KeV)
180
90
0
PITCH ANGLE (DEG)
905300
905310
905320
905330
TIME (SEC)

Figure 4

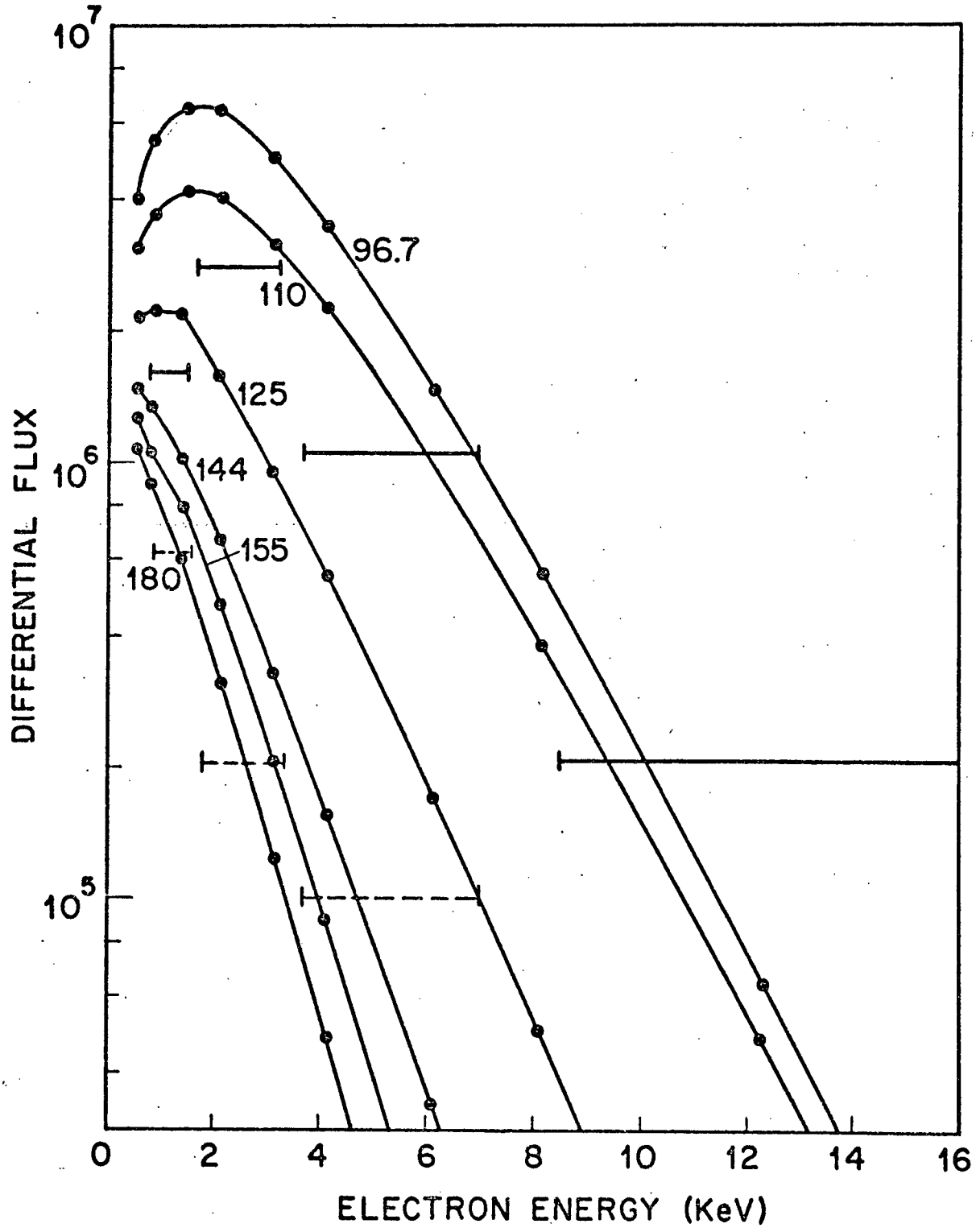
10^7
10^6
10^5
DIFFERENTIAL FLUX
96.7
110
125
144
155
180
0
2
4
6
8
10
12
14
16
ELECTRON ENERGY (KeV)

Figure 5

Chapter II

SUBSTORM EFFECTS IN AURORAL SPECTRA

Introduction

High latitude geophysical data are almost always displayed in a system of invariant latitude and magnetic time. Usually the aim of such an organization is to produce a systematic separation of the various regions of the magnetosphere as reflected by the statistical properties of the geophysical data. Because of the high latitude phenomena is governed largely by the magnetic field of the Earth, the coordinata system of invariant magnetic latitude and magnetic time is generally a good choice.

The magnetosphere is known to undergo large morphological changes as a function of geomagnetic activity and the coordinata description must allow for the shifts of the various boundaries. This is clearly evident for example by the motion of the auroral zones to lower latitudes at the time of high activity (Feldstein and Starkov, 1968) as represented by K_p. Attempts have been made to incorporate these gross latitudinal shifts of the auroral phenomena with varying K_p into a coordinate system (Starkov, 1969). Such "oval latitude" has been used to systematize photometric data by Eather and Mende (1972) by using the calculated equatorial boundary of the oval as a base line.

It has been recognized that large scale magnetospheric configurations occur during substorms on very short time scales (Akasofu, 1968). The previous analyses of Eather and Mende (1971, 1972) according to invariant latitude, time and three hour K_p index represent an average over all phases of substorms and thus do not present any of the substorm dependent effects in the optical aurora.

In these previous analyses of airborne photometric data, we have derived average latitudinal distributions of particle type, flux and energy of the day and night side and were able to delineate distinct zones of precipitation of various particle population which allowed meaningful identification with magnetospheric source regions. The results of this analysis thus represent a mean picture averaged over all phases of substorms. It tells us very little for example about the changes which occur due to substorms in the latitudinal distribution of the precipitation in terms of particle type, flux and energy and therefore does not allow the identification of any substorm related changes.

The magnetic activity dependent latitude coordinata helped the ordering of the data and the question arises whether one should look for a substorm dependent time coordinata which would further order the data. If a suitable coordinata system were found, the performance of the analysis similar to Eather and Mende's, 1970 and 1971, using the substorm time related coordinata system might clarify the invariant latitude and magnetic time location of the boundaries of the various precipitation regions during the various phases of the substorm. The work following is an attempt to perform such an analysis.

TABLE 1

MAGNETIC OBSERVATORIES USED TO IDENTIFY SUBSTORMS AND MAGNETIC STORMS

STATION	GEOMAGNETIC CO-ORDINATES	
	Latitude	Longitude
Lerwogur	70.2	71.0
Kiruna	65.2	115.6
Sodankyla	63.8	120.0
Yakutsk	50.9	193.8
College	64.6	256.5
Victoria	54.2	293.0
Meanook	61.8	301.0
Baker Lake	73.8	315.3
Churchill	68.7	322.8
Great Whale	66.6	347.4
Ottawa	56.8	351.5
Honolulu	21.1	266.8
Tuscon	40.4	312.2
Dallas	42.9	327.7
Fredericksburg	49.6	349.8

Substorm Time

The auroral substorm concept has been the most important development in magnetospheric and auroral physics during the past few years. There have been many ground-based and satellite studies of all phases of the substorm, and considerable arguments in the literature on whether or not there is a growth phase that involves systematic charges in measurable parameters such that one can confidently say a substorm is imminent.

The expansive phase of a substorm is readily identified if one has good magnetometer coverage both in latitude and local time. The substorm however is only detected over a restricted latitude and time interval, the size of the area of detection depending on the strength of the substorms. There is almost always a number of substorms in any given 24 hour period, and these will usually be detectable at one or more of the network of ground-based observatories. However, because of the incomplete coverage of the ground-based observations, it is possible that some substorms will go undetected by all observatories.

We define a substorm time coordinata system in which the origin is at the time T_s(UT) which is the first observation of the auroral zone negative bay associated with the particular substorm. Thus, the time coordinata of an observation occuring at time T (UT) will be T - T_s in the substorm time coordinata system.

Magnetic records for the 14 observatories shown in Table 1 were collected for the five months (Jan.-March, 1968; Nov.-Dec., 1969) during which the NASA Airborne Auroral expeditions took place. All

magnetograms from 6 hours before the beginning of airborne observations to 6 hours after the end of observations were examined for the occurrence of substorms. An example of a substorm identification is shown in Figure 1. The substorm was identified to occur at 0600 UT earliest on the Ft. Churchill magnetogram. For comparison several mid-latitude magnetic stations are also shown. Interesting to note that the identification of substorm is often possible from midlatitude magnetograms because of the simultaneous onset of large scale magnetospheric currents. It was usually possible to clearly identify a substorm within the time period examined for each flight, and there were often two and sometimes three different substorms in the period.

The photometric data previously analyzed is in the form of two-minute averages of zenithal emission intensities. Some 3860 data points were available; of these, some 3180 were associated with flights where substorm(s) were identified before, during or after the flight, and some 680 could not be associated with a detected substorm.

(a)

OVAL LATITUDE INTERVAL (degrees)

	<-1½	-1½	-1	-½	0	½	1	1½	>1½
12									
10	1.6	0.9	0.7	2.8	3.9			1.5	
8	1.7	0.7	1.1	2.5	2.3	1.9	2.8	1.8	
6	0.9	1.4	2.5	1.4	2.8	2.3	3.0	2.1	
4	1.4	1.4	2.1	1.4	3.8	3.8	4.2	2.8	
2	2.2	1.1	1.6	1.6	3.6	5.4	3.9	3.9	
0	1.9	1.3	1.9	1.3	2.6	1.7	2.6	2.4	
-2	2.2			1.3	2.1	1.9			
-4				1.8	3.0				

SUBSTORM TIME (HOURS)

(b)

OVAL LATITUDE INTERVAL (degrees)

	<-1½	-1½	-1	-½	0	½	1	1½	>1½
12									
10	1.1	1.0	0.3	3.9	2.6		1.2	1.9	
8	1.1	0.9	1.7	3.4	1.7	1.9	1.6	2.2	
6	1.6	1.2	3.9	3.6	1.8	1.8	2.6	2.3	
4	2.6	2.3	2.9	2.1	2.0	2.0	2.9	2.2	
2	2.7	5.1	1.5	1.6	2.1	3.1	2.4	2.4	
0	1.6	5.1	1.3	2.0	2.1	3.0	2.2	3.1	
-2	2.0				1.7		6.6	4.0	
-4	3.2							4.9	

HOURS FROM MIDNIGHT LMT

TABLE 2

Spectral parameter α (kev) for precipitating electrons, averaged over the indicated latitude and time intervals

Results

Photometric spectral ratios were used to determine the characteristic energy, α, of precipitating electrons. In the determination of α (Eather and Mende, 1972; Mende and Eather, 1972) the electron energy spectrum of the form $N(E)dE = N_o E_e^{-E/\alpha} dE$ is used. Thus, α is twice the mean energy $\bar{E}$. The average values of α are given in the oval latitude and substorm time boxes are indicated in Table 2a. If there were less than ten data points in a box, then no average is indicated. The most obvious feature is the hardening of the precipitation spectrum in the 1/2 hour interval after substorm onset.

For comparison, the same data are presented as functions of local magnetic time in Table 2b. Now there are no obvious trends evident, and it becomes immediately evident that substorm time may be a valuable ordering parameter.

The average energies shown in Table 2 are not particularly meaningful because events with high α contribute more to the average than events with low α. Consequently, a more useful presentation is to consider the percentage occurrence of α exceeding a given energy; as in our previous paper, we considered the percentage of times α exceeded 5 kev, i.e. a fairly hard precipitation spectrum.

Percentage occurrence histograms for $\alpha > 5$ keV are shown in Figure 2, where an average has been performed over all oval latitudes. The plot against substorm time (Figure 2a) shows a definite probability for spectral hardening at the time of and following a substorm. As substorms tend to occur near local magnetic midnight, one might expect a similar trend to be evident when the data are plotted against magnetic time.

Figure 2b shows, however, that this is not the case, and no trends at all emerge from such a presentation.

In Figure 3 the same data have been broken up into 2° boxes of oval latitude, with consequently poorer statistics. Where a low percentage occurrence is plotted (1%), it indicates there were more than five data points in the box and indeed the percentage occurrence was $\leq 1\%$. A zero percentage occurrence on the histograms indicates less than five data points so an average was not performed. The same trend of a hardening of the spectrum just after a substorm is evident in the oval latitudes $\geq 2^{\circ}$. Within $\pm 2^{\circ}$ of the equatorial edge of the auroral oval (0° oval-latitude), such a trend is not evident, but rather a hardening does not become apparent until about an hour after the substorm. We suspect this reflects the poleward expansion of the aurora during substorms, so that it is not until the recovery phase when the aurora returns to the typical oval position, that the higher-energy substorm electrons are detected at these latitudes. However, lack of better statistics precludes any strong conclusions on this point.

If there were sufficient data points over the complete grid of oval latitudes and substorm time, it would be interesting to further classify the data according to the local time of the observation. This would then give a complete spatial picture (over latitude and local time) of the characteristics of electron precipitation at various substorm times. (If we chose 2° latitude intervals from -4° to 12°, 2 hour local time intervals from 1800 to 0600, and 1/2 hour substorm time intervals

for -1 1/2 to +1 1/2 hours, this would involve some 288 boxes to order the data, and with current data we simply do not have enough coverage.

As a first step in this direction, Figure 4 shows the same data as Figure 3, but subdivided further into evening (1800-0000) and morning (0000-0600) hours. The evening plots again show the definite hardening of the precipitation at the time of substorm, and that this harder spectrum persists from > 1 1/2 hours after substorm onset.

The morning plot was a surprise in that it indicates the abrupt increase of electron energy at substorm onset is mainly a feature of the evening sector. The hardening does not become apparent in the morning sector until about one hour after substorm onset. This could be consistent with particle injection on the evening side of the geomagnetic midnight, with consequent trapping of some electrons and curvature drift to the morning section. For example, at L = 8, 10 keV electrons will drift about 2 1/2 hours in local time in one hour elapsed time, and this will move them from an injection point just before midnight to a region well into the morning sector. Again, we do not feel confident enough of our statistics to make strong conclusions on this point.

Conclusions

The conclusions in terms of the delineation of substorm processes from this analysis are not particularly new or surprising. The general hardening of electron precipitation after a substorm is well known; the data of Figure 3 fit into the well-known picture of poleward expansion of aurora during a substorm; and the data of Figure 4 indicating injection on the evening side of midnight and consequent curvature drift of electrons is also not a surprising result.

The main point we would like to emphasize from this analysis is the usefulness of substorm time as a time coordinate. In fact, most of the conclusions summarized in the previous paragraph would not have been evident from an analysis that used magnetic time as a time coordinate. There has been an increasing trend in the literature to relate measurements to the time of substorm occurrence. This involves the tedious business of collecting and examining magnetograms from a large number of observatories but analyses such as those presented here indicate that it is a worthwhile, if not necessary, procedure. It would be nice to see some organization assume the responsibility for this and publish monthly summaries of substorm occurrences (both time of onset and local time sector of maximum amplitude).

Acknowledgements

The 1968 and 1969 NASA Airborne Expedition was managed by the Airborne Sciences Office, Ames Research Center. This expedition provided the data base for this work. Special thanks are due to Mr. L.C. Haughney of the Airborne Science Office and Dr. M. Dubin of NASA Headquarters for their continued interest in the progress of the auroral data analysis.

LIST OF FIGURES

Figure 1 The identification of a substorm from the collection of magnetic stations indicated in Table 1. The auroral zone negative bay is indication of the onset of the expansive phase. The midlatitude positive "recovery" also indicates the onset of the substorm. The substorm time zero was identified as 0600 UT for this substorm.

Figure 2a Histogram of percentage occurrence of auroras of characteristic energy, α, greater than 5 keV. 100% is the total number of auroral observations (4278 N_2^+ emission greater than 0.5 Rayleighs) in any substorm time box.

Figure 2b The same data in terms of local magnetic time boxes.

Figure 3 Percentage occurrence of auroras of characteristic energy, α, greater than 5 keV separated in oval latitude and substorm time. 100% is referred to the total number of auroral observation (4278 N_2^+ greater than 0.5 Rayleighs) in box.

Figure 4 Percentage occurrence of auroras of characteristic energy, α, greater than 5 keV separated according to substorm time for pre-midnight local time and post midnight local time hours.

References

Akasofu, S.I.; Polar and Magnetospheric Substorms, p. 27, Springer, New York, 168.

Eather, R.H. and S.B. Mende; "Airborne Observations of Auroral Precipitation Patterns," J. Geophys. Res. 76, 1746, 1971.

Eather, R.H. and S.B. Mende; "Systematics in Auroral Energy Spectra," J. Geophys. Res. 77, 660, 1972.

Feldstein, Y.I. and G.V. Starkov; "Auroral Oval in the IGY and ISGY Period and Ring Current in the Magnetosphere," Planet. Space Sci., 16, 129, 1968.

Mende, S.B. and R.H. Eather; "Photometric Auroral Particle Measurements," Earth's Magnetospheric Processes, ed. B.M. McCormac, pp. 179-186, D. Reidel, Dordrecht, Holland, 1972.

Starkov, G.V.; "Analytical Representation of the Equatorial Boundary of the Auroral Zone," Geomagn. Aeron., 9, 614, 1969.

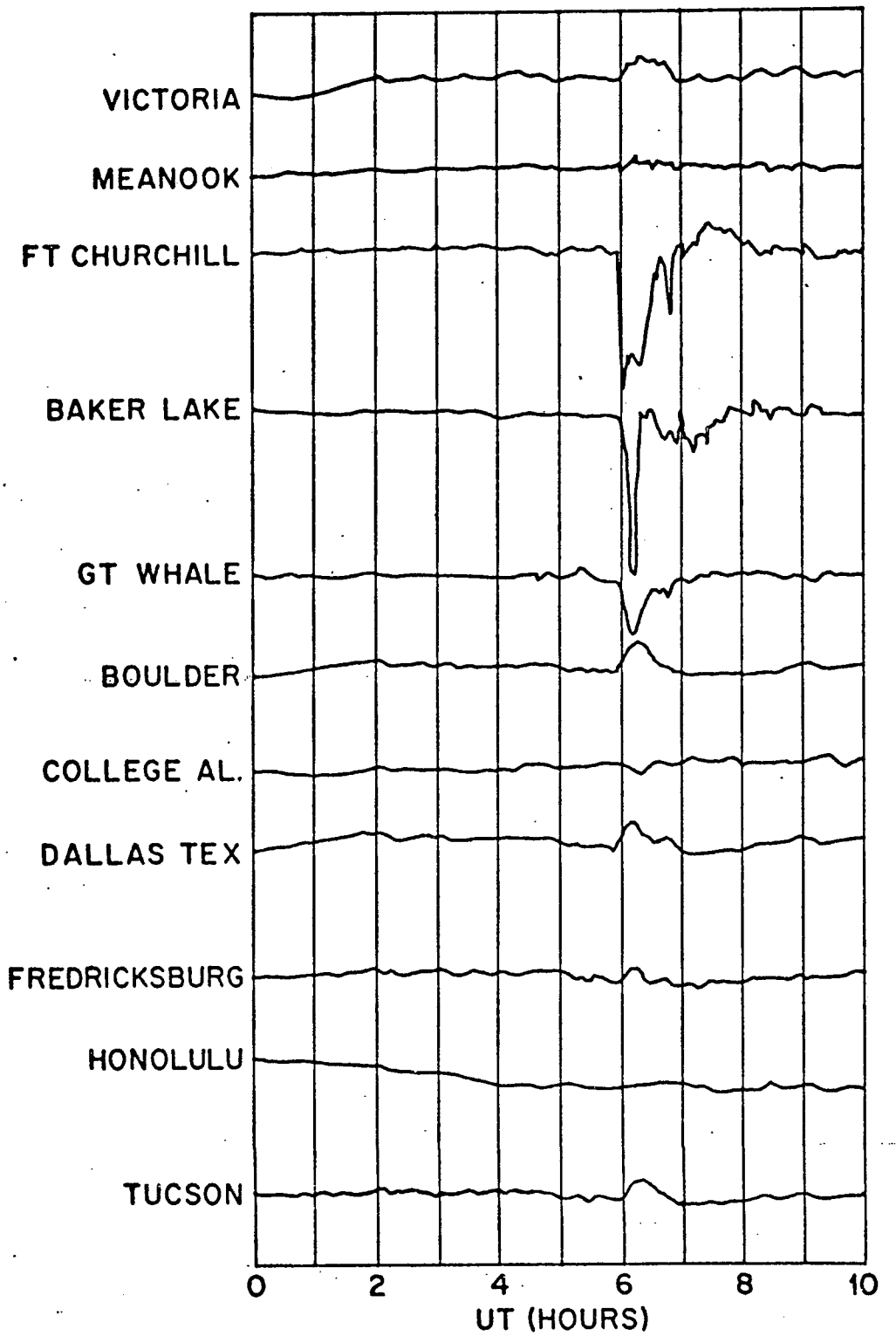
VICTORIA
MEANOOK
FT CHURCHILL
BAKER LAKE
GT WHALE
BOULDER
COLLEGE AL.
DALLAS TEX
FREDRICKSBURG
HONOLULU
TUCSON
0
2
4
6
8
10
UT (HOURS)

Figure 1

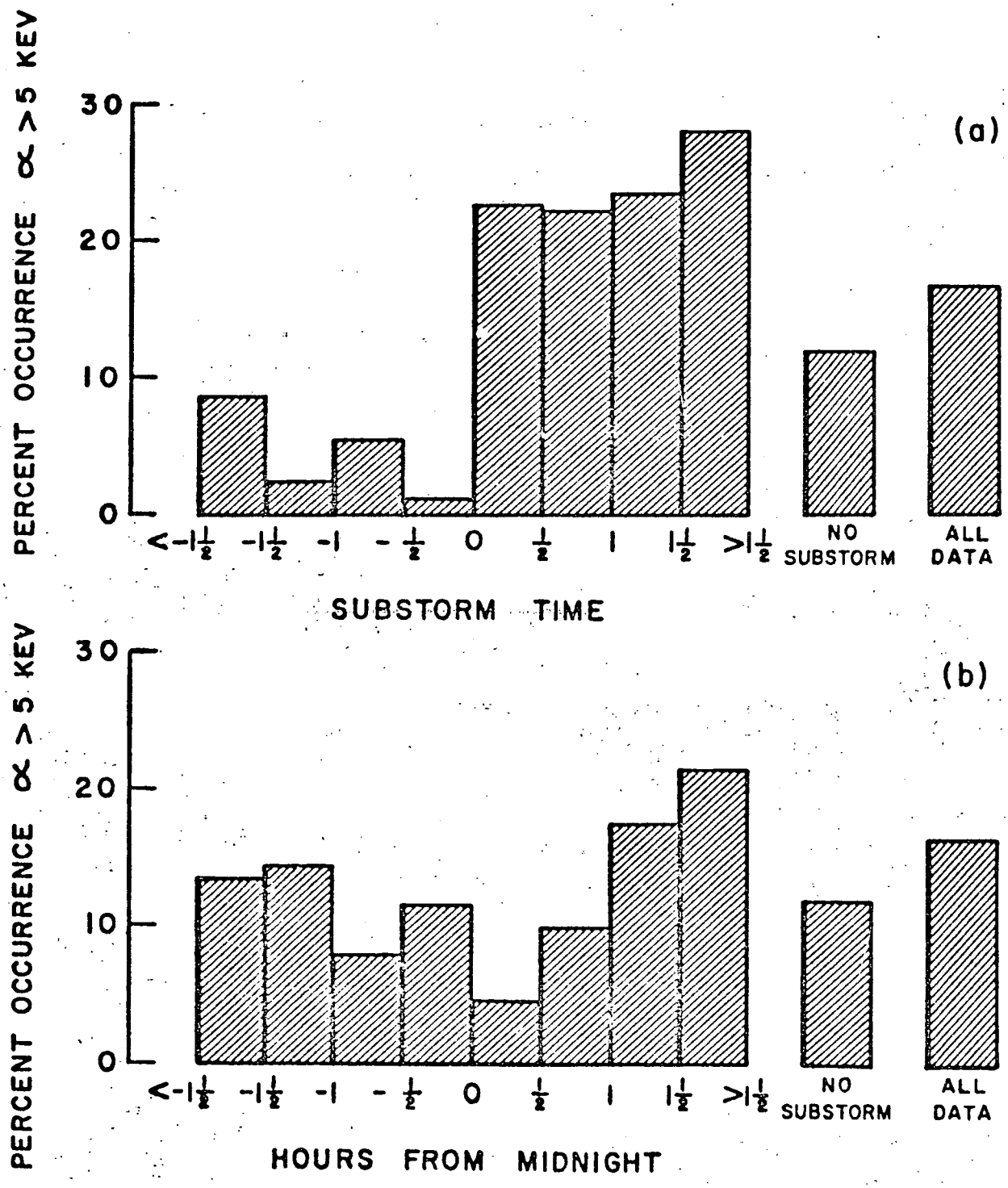
PERCENT OCCURRENCE ∝ > 5 KEV
30
20
10
0
(a)
<-1½
-1½
-1
-½
0
½
1
1½
>1½
NO SUBSTORM
ALL DATA
SUBSTORM TIME
PERCENT OCCURRENCE ∝ > 5 KEV
30
20
10
0
(b)
<-1½
-1½
-1
-½
0
½
1
1½
>1½
NO SUBSTORM
ALL DATA
HOURS FROM MIDNIGHT

Figure 2

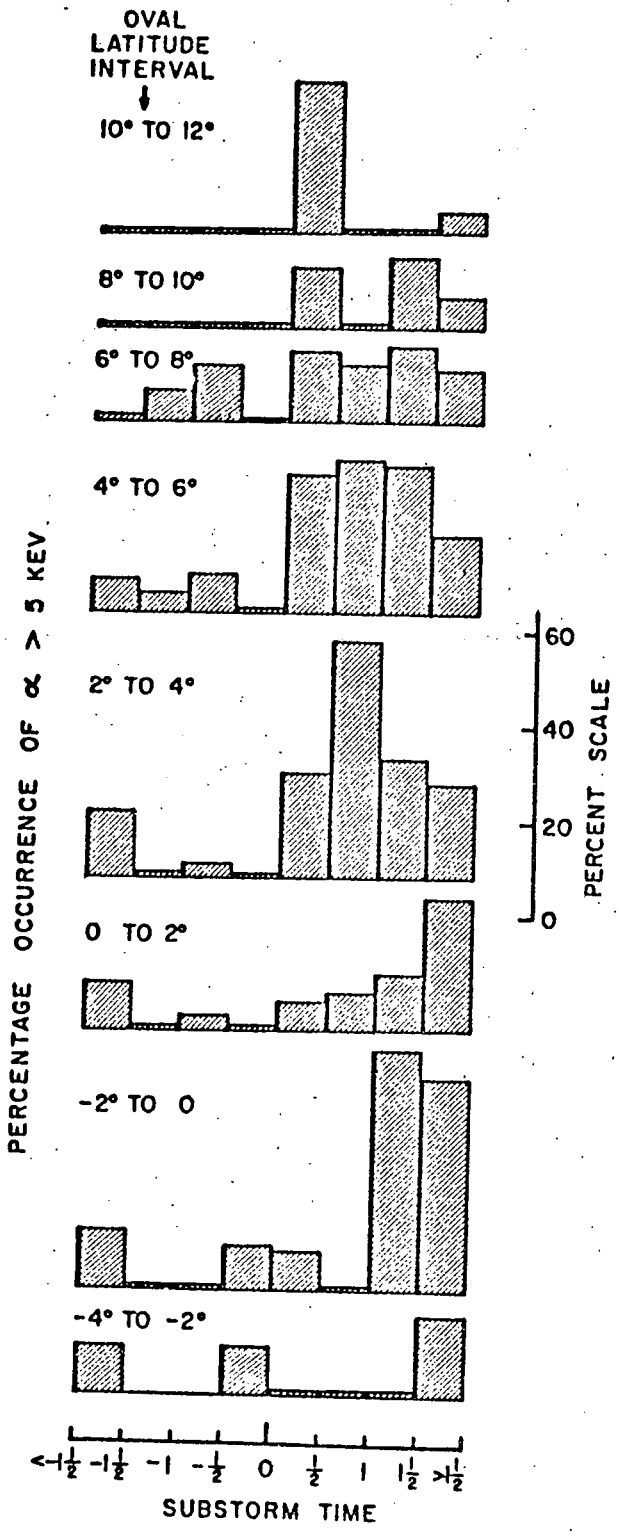
OVAL
LATITUDE
INTERVAL
10° TO 12°
8° TO 10°
6° TO 8°
4° TO 6°
2° TO 4°
0 TO 2°
-2° TO 0
-4° TO -2°
PERCENTAGE OCCURRENCE OF α > 5 KEV
60
40
20
0
PERCENT SCALE
<-1½ -1½ -1 -½ 0 ½ 1 1½ >1½
SUBSTORM TIME

Figure 3

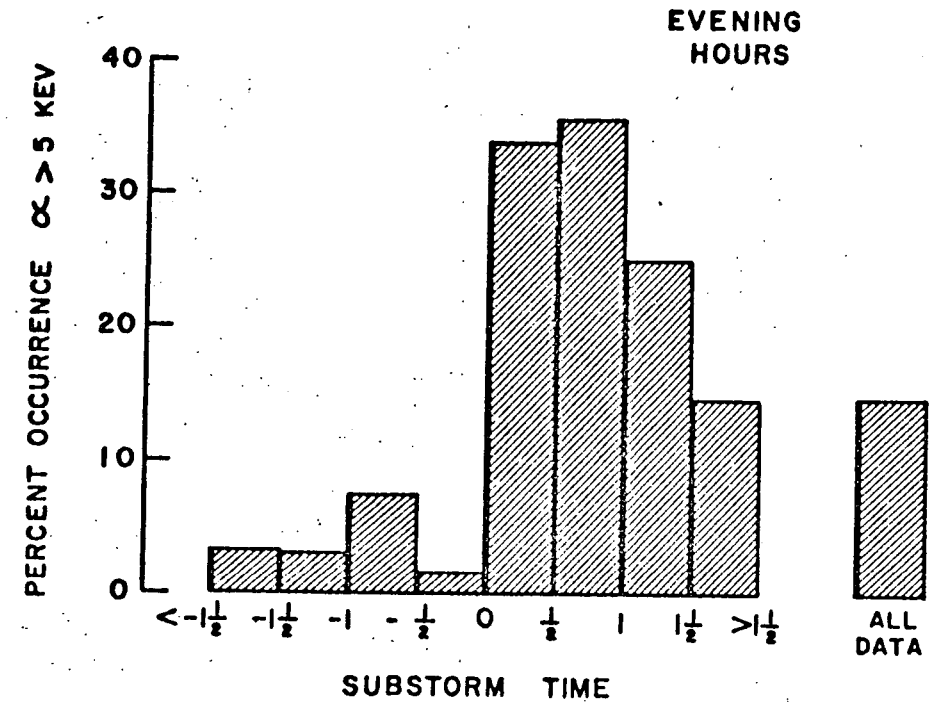
EVENING
HOURS
PERCENT OCCURRENCE ∝ >5 KEV
40
30
20
10
0
< -1½
-1½
-1
- ½
0
½
1
1½
>1½
ALL
DATA
SUBSTORM TIME

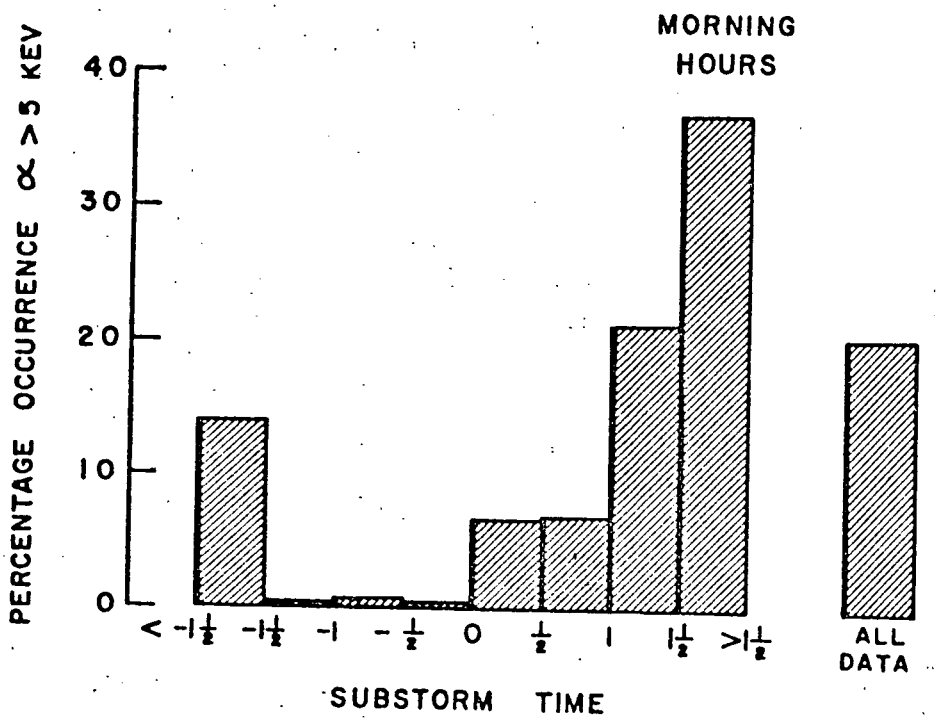
MORNING
HOURS
PERCENTAGE OCCURRENCE ∝ >5 KEV
40
30
20
10
0
< -1½
-1½
-1
- ½
0
½
1
1½
>1½
ALL
DATA
SUBSTORM TIME

Figure 4